Biotypes of deeply phenotyped depressed patients reflect signatures of adverse childhood experience and depressive cognitive biases

Federica Colombo[1*], Federico Calesella[1], Beatrice Bravi[1], Lidia Fortaner-Uyà[1,2], Camilla Monopoli[1], Tommaso Cazzella[1,2], Michele Acconcia[1], Raffaella Zanardi[2,3], Cristina Colombo[2,3], Matteo Carminati[1], Chiara Fabbri[4], Alessandro Serretti[5], Irene Bollettini[1], Francesco Benedetti[1,2], Sara Poletti[1,2], Benedetta Vai[1,2]

1 Psychiatry and Clinical Psychobiology Unit, Division of Neuroscience, IRCCS San Raffaele Hospital, Milan, Italy

2 University Vita-Salute San Raffaele, Milan, Italy

3 IRCCS San Raffaele Hospital, Mood Disorders Unit, Milan, Italy

4 University of Bologna, Department of Biomedical and Neuromotor Sciences, Bologna, Italy

5 Department of Medicine and Surgery, Kore University of Enna, Enna, Italy

***Corresponding author:** Federica Colombo (colombo.federica@hsr.it)

Sara Poletti and Benedetta Vai are co-senior authors.

Running title: Cognitive biases in trauma-related depressive biotypes

Keywords: Depression, Adverse Childhood Experience, Cognitive Biases, Machine Learning, Neuroimaging, Biotypes

Abstract

Background: Negative Cognitive Styles (NCS) are key features of depression contributing to severe clinical outcomes by sustaining negative affect. However, depression is clinically heterogeneous, reflecting complex neurobiological and environmental interactions. Characterizing heterogeneity using multimodal data could help identify mechanisms mapping onto different phenotypes and discover high-impact biomarkers.

Methods: Using a stability-based relative clustering validation pipeline, 344 depressed patients (135 major depressive disorder, 209 bipolar disorder) were stratified based on multimodal neuroimaging data, including grey matter volumes, cortical thickness, white matter diffusivity indices, resting-state functional connectivity (FC), and spontaneous neural activity. Clusters were derived from each modality separately and in combination, and profiled for Adverse Childhood Experiences (ACEs) and NCS.

Results: All neuroimaging modalities stratified depressed patients into two clusters, with the FC-based model achieving the highest accuracy (85%). Compared with healthy controls (HC, N=138), these clusters exhibited opposite patterns of global functional hyper-integration (Cluster 1) and hyper-segregation (Cluster 2). Unique multivariate neurobiological-ACEs relationships characterized the FC-based clusters. While ACEs negatively affected FC in Cluster 1 and HC, Cluster 2 showed opposite effects specific to ACE subtypes, with sexual abuse positively influencing FC. Mediation analysis showed that FC strength mediated the relationship between ACEs and NCS of overgeneralize only in Cluster 2. ACE-related functional alterations pinpoint brain regions involved in socioemotional and cognitive development, sensitive to maturational neural changes.

Conclusions: These findings provide evidence of clinically meaningful depression "biotypes" shaped by ACEs and associated with NCS, underlining the feasibility of computational psychiatry tools to uncover data-driven patterns for precision psychiatry.

Introduction

Depressive disorders carry a substantial social and economic burden, demanding more personalized and effective clinical strategies (1,2). Negative Cognitive Styles (NCS) - including dysfunctional attributional styles and negative thinking – are key prognostic factors in the onset and maintenance of depression (3). NCS are associated with poor therapeutic responses and increased suicidality (4–6), while targeted interventions can improve clinical symptoms and overall functioning (7–9). Identifying the factors that influence and moderate NCS is of critical importance, particularly given the substantial heterogeneity in how patients respond to treatments (10).

Adverse Childhood Experiences (ACEs) are critical environmental contributors to mood disorders, interacting with genetic predispositions to shape clinical trajectories (11). Individuals exposed to ACEs often experience a worse illness course, including poor treatment response and increased suicidality (12–14). Cognitive theories of depression propose that ACEs foster NCS by shaping early maladaptive cognitive patterns (3). This pathway could be potentially driven by ACEs-related structural and functional brain alterations (15), which primarily impact networks governing emotion regulation, threat detection, and cognitive functions (16,17). Exposure to ACEs was indeed shown to affect neural correlates specifically associated with psychiatric conditions, including grey matter (GM) volumetric reductions and white matter (WM) disruption (18–23).

Understanding how these factors moderate and predict clinical outcomes is a primary objective of precision psychiatry (24–26). However, these interactions are unlikely to be consistent across patients, reflecting transdiagnostic heterogeneity (27). Recent research has identified neurobiological subtypes (i.e., biotypes) of depression, offering a data-driven stratification to better capture clinical and biological diversity. For instance, increased default mode network functional connectivity (FC) was linked to a "rumination" biotype (28–30), while heightened activity within the cognitive control circuit predicts negative biases and treatment response (31). Nevertheless, stratification studies have predominantly relied on resting-state functional MRI (32–35), leaving the structural basis largely unexplored. We recently identified distinct biotypes of major depressive disorder (MDD) using structural neuroimaging: one marked by reduced GM, cortical thickness (CT), and WM integrity - linked to anergy, childhood abuse, and inflammatory markers - and another with more preserved structure, associated with cognitive symptoms (e.g., negative self-esteem) (36). However, exploring interactions between ACEs and NCS in different biotypes for multimodal neuroimaging data remain unaddressed.

In this study, we applied an unsupervised machine learning approach to stratify depressed MDD and bipolar disorder (BD) patients using structural, functional, and multimodal neuroimaging. We then examined the neurobiological and clinical features of each cluster, focusing on the relationships between NCS, ACEs, and neural correlates. Finally, we explored whether ACEs-related brain signatures mediates the relationship between ACEs and NCS using multivariate models, which are well-suited to capture complex brain-behavior associations underlying psychiatric heterogeneity (27,37).

Methods and Materials

Participants

The sample included 344 inpatients (135 MDD, 209 BD), consecutively admitted at the IRCCS San Raffaele Hospital (Milan, Italy) and diagnosed according DSM-5 criteria using the Structured Clinical Interview for the Diagnosis of Axis I Disorders (SCID-5). Inclusion criteria were age 18-65 years old and current depressive episode. Depression severity was assessed with the 21-items Hamilton Depression Rating Scale (HDRS-21) (38). Exclusion criteria for all patients included: major medical and neurological disorders, pregnancy, intellectual disability, history of drug or alcohol abuse or dependency, and psychiatric comorbidity on axis I. A sample of 138 healthy controls (HC) without psychiatric history or first-degree familial risk was also recruited. MRI acquisitions were performed for all participants between 2.30 pm and 6.00 pm. After a complete description of the study, written informed consent was obtained. All procedures contributing to this work comply with the ethical standards of the relevant national and institutional committees on human experimentation and with the Helsinki Declaration of 1975, as revised in 2008. The study was approved by the local ethical committee.

Sociodemographic, childhood trauma and cognitive styles measures

Age, sex, number of previous mood episodes, age of onset, duration of illness, and years of education were collected. Medication load was calculated for each subject categorizing each medication into 0-4 scores based on dose range, and then combined to obtain a single composite score (see **Methods S1** for detailed criteria) (39). In a subsample of 229 patients (106 MDD, 123 BD) and 98 HC, childhood trauma was assessed through the 28-item version of the Childhood Trauma Questionnaire (CTQ) (40), which investigates 5 categories of childhood trauma: physical, emotional, and sexual abuse; physical and emotional neglect. Each form of maltreatment is evaluated through 5 items, where high scores reflect higher exposure (40). NCS were assessed through the Cognition Questionnaire (CQ) (41), which provides a fine-tuned evaluation of negative thinking in response to positive, neutral, and negative events (41). Five different dimensions of NCS can be derived: emotional impact, attribution of causality, generalization across time, generalization across situations, and perceived uncontrollability. High scores in each domain reflect high degree of that specific cognitive distortion.

MRI data acquisition, processing and features extraction

The acquisition of T1-weighted, diffusion tensor imaging (DTI), and resting-state fMRI images was performed with two different 3.0 Tesla scanners. Details about acquisitions parameters for each scanner are reported in **Methods S2**.

The processing of T1-weighted neuroanatomical images was performed through the Computational Anatomy Toolbox (CAT12) for statistical parametric mapping (SPM) software (42). The main pre-processing steps involved: normalization in the Montreal Neurological Institute (MNI) space; tissue segmentation into GM, WM, and cerebrospinal fluid (CSF); check of spatial alignment and sample homogeneity to exclude outliers; spatial smoothing of each GM map with a 6 mm full width at half maximum Gaussian filter. CT was computed

for 68 regions derived from the Desikan-Killiany atlas (43), while cortical and subcortical regional volumes were extracted for 122 regions identified from the Neuromorphometrics atlas (http://Neuromorphometrics.com/). The total intracranial volume (TIV) was also computed.

DTI pre-processing was performed using FMRIB Software Library (FSL) 6.0 tools (44–46). All images were corrected for eddy currents and head motion (47) and skull-stripped (48). Non-linear registration to the FMRIB58-FA template was performed, and a diffusion tensor model was fitted at each voxel to obtain voxel-wise maps of fractional anisotropy (FA), axial (AD), radial (RD), and mean diffusivity (MD). The obtained images were then processed using FSL's Tract Based Spatial Statistics analytic method and aligned to the MNI space through the Non-Linear Image Registration Tool (FNIRT). For each DTI index, the maps of all subjects were merged into a common 4D image, and a "thinning" process was applied to create a skeletonized mean image representing the centers of all common tracts. A threshold of 0.2 was set for this image to control for inter-subject variability and reduce the likelihood of a partial volume effect. Whole-brain tract-based average values for each diffusion index were extracted according to ENIGMA-DTI protocols. Average FA values were calculated from voxels in each subject's white matter skeleton within 43 tract-wise ROIs, derived from the Johns Hopkins University parcellation atlas (49). The same procedure was performed for the extraction of tract-based average values of AD, RD and MD. All measures were separately calculated for the right and left hemispheres in each tract, except for midline structures.

The T2*-weighted images were analyzed using the Harmonized AnaLysis of Functional MRI pipeline (HALFpipe) version 1.2.1 (50). Pre-processing steps encompass motion correction, slice time correction, susceptibility distortion correction, coregistration, and spatial normalization to the MNI152NLin2009cAsym template. Denoising was performed on the resampled images and included: spatial smoothing with a 6 mm full-width at half-maximum kernel; grand mean scaling of 10,000; ICA-AROMA (51,52); and temporal filtering using a Gaussian weighted high-pass (width of 125 s) for FC and a frequency-based bandpass (0.01-0.1 Hz) for measures of local neural activity. Physiological nuisance regressors were isolated for anatomical component correction (aCompCor) considering the top 5 CSF principal components (53). Several resting-state fMRI features were calculated. Considering FC, the time series from 246 Brainnetome (54) and 17 cerebellar regions of interest (ROIs) were extracted (55). ROIs with missing time series across participants were excluded, resulting in 186 ROIs (**Table S1**). From the individual ROI-to-ROI FC matrices, positive (Spos) and negative (Sneg) strengths (i.e., the sum of positive and negative weights of links connected to a region) were computed for each ROI using the Python-equivalent of the Brain Connectivity Toolbox (bctpy, https://github.com/aestrivex/bctpy). Local activity metrics included the fractional amplitude of low frequency fluctuations (fALFF) and regional homogeneity (ReHo), calculated from the pre-processed images. fALFF was defined as the ratio of low frequencies (0.01–0.1 Hz) to the entire frequency power (56). ReHo measures the temporal synchronization of a voxel with its nearest neighboring voxels, calculated using the Kendall's coefficient of concordance (57). Voxel-wise fALFF and ReHo maps for each participant were Z-standardized, and the corresponding average values across 186 ROIs were extracted.

To account for inter-scanner variability, ComBat harmonization (58) was performed for each neuroimaging

feature using neuroCombat (https://github.com/Jfortin1/ComBatHarmonization/tree/master), considering age, sex, diagnosis, and TIV (for GM and CT) as biological covariates to be preserved.

Unsupervised machine learning analysis

To uncover biologically-driven subtypes of depression, a stability-based relative clustering validation algorithm (*NeuReval* Python package) (36,59) was implemented for each neuroimaging modality (**Figure 1B**). This method leverages cross-validation to evaluate clustering generalizability by embedding unsupervised clustering in a supervised learning framework (60). For all the models, input features were standardized, and confounding effects (age, sex, pharmacological load, frequency of episodes, and TIV for GM and CT) were regressed out, including age² and age-by-sex interaction to account for non-linear effects (61). All these steps were fitted on the training set and then applied to the test set. A 2-fold cross-validation scheme (50% training, 50% test) was employed to account for size imbalances resulting from training-test sets splitting (59), and it was repeated 100 times to ensure robustness. For all the models, K-Means was implemented for clustering, while Support Vector Machine (SVM) served as supervised classifier. A grid search procedure was performed for hyperparameters tuning, using the minimization of the normalized stability as the criterion to select the optimal ones. These included K-Means initialization (random or k-means++), the soft-margin C (range: 0.01, 0.1, 1, 10, 100, 1000), and kernel type (linear or radial basis function) for SVM. Clustering solutions were evaluated for 2 to 5 clusters, and the one achieving the minimum normalized stability throughout cross-validation was selected.

To investigate whether the combination of different neuroimaging modalities improved stratification over single-modality models, a multiview spectral clustering algorithm was embedded within the *NeuReval* pipeline (https://github.com/fede-colombo/Multiview_NeuReval). In multiview frameworks, different feature sets ("views") are entered within the clustering algorithm, which can be separately used to derive clusters. The rationale behind this approach is that the grouping structure identified in one view should agree with the one derived from another view. The best clustering solution is the one that assigns an observation to the same cluster regardless of the specific view (62). Only modalities that resulted in stable solutions in single-modality models were included, considering the same cross-validation scheme and confounds controls. Tuned hyperparameters included the affinity matrix (radial basis function or nearest neighbors) for multiview spectral clustering and SVM hyperparameters.

The internal quality of clustering solutions was further assessed with the Silhouette score and the Davies-Bouldin index. Statistical significance was tested with 10,000 Monte Carlo simulations using the *sigclust* method (R library) (63). Only stratification models that passed false-discovery rate (FDR) $q<0.05$ threshold were deemed as significant.

Univariate and multivariate characterization of the clusters

For each significant model, clusters were compared for age, diagnosis, sex, number of previous episodes, years of education, age of onset, duration of illness, pharmacological load, HDRS-21 total score, CTQ and CQ total

scores and domains. The same approach was employed for neuroimaging features. Cohen's d effects sizes were calculated and multiple comparisons were FDR-corrected ($q<0.05$). Comparisons with HC were conducted only for the best-performing model. Cluster assignment agreement across models was assessed with the Fleiss' kappa statistic.

For each significant stratification model, grouped partial least squares correlation (PLSC) analyses were also performed to investigate whether the multivariate neurobiological-ACEs relationship was different between clusters (myPLS MATLAB toolbox, https://github.com/danizoeller/myPLS/). (**Figure 1 D-E**). PLSC is a multivariate technique that identifies latent variable (LV) pairs capturing shared variance between two datasets (e.g., brain and behavioral data). With group labels, PLSC computes separate covariance matrices, enabling detection of between-cluster differences in multivariate brain–behavior associations (64). Prior to analyses, neuroimaging variables were residualized for the same confounds considered for *NeuReval*. CTQ scores were adjusted for age, sex, and education. For each model, 5000 permutations were performed to assess the statistical significance of the LV pairs (FDR $q<0.05$). Brain bootstrap ratio (BSR) and 95% confidence intervals (CI) on neurobiological-ACEs correlations were estimated through 5000 bootstrap resampling. BSRs were computed by dividing the correlation coefficient for each biological variable by its bootstrapped standard deviation, and interpreted as standardized weights (64). BSRs>|2| were judged as important in guiding the neurobiological-ACEs relationships, whereas CTQ loadings with 95% CI that do not include zero were deemed as significant. BSRs were converted into p-values and FDR-corrected ($q<0.05$) (65).

For significant LV pairs, multivariate general linear models (GLMs) were implemented separately for each cluster, with LV neurobiological scores predicting CQ domains. Univariate analyses were also performed within each cluster to explore the effect of LV neurobiological scores on each CQ domain. Statistical significance was assessed using parametric estimates of the predictor variables, calculated by the least squares method. For those CQ domains that were significantly predicted by LV neurobiological scores, mediation models were performed, considering LV CTQ scores as independent variables, LV neurobiological scores as mediator, and CQ domain as dependent variable (5000 bootstraps, 90% CI) (SPSS PROCESS macro) (66). (**Figure 1F**).

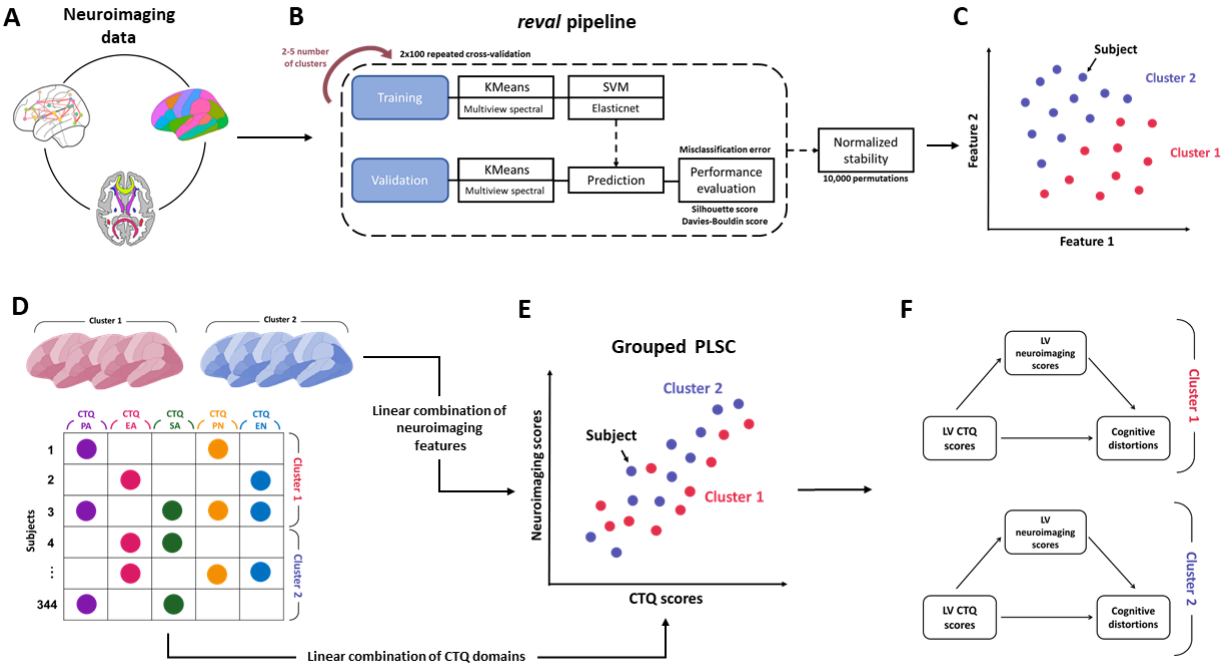

Figure 1. Graphic representation of the analysis pipeline. *A. Neuroimaging data were extracted for each subject. B-C. For each type of feature, a stability-based relative clustering approach was implemented. The best clustering solution was identified minimizing the misclassification error (i.e., normalized stability). D-E. For each stratification model, multivariate neurobiological-ACEs relationships were investigated through Partial Least Squared Correlation (PLSC) in each cluster. F. For significant latent variables (LV), mediation analyses were performed to investigate the mediating effect of LV neurobiological scores on the relationship between LV CTQ scores and Cognition Questionnaire (CQ) domains in the discovered clusters. Abbreviations: SVM, support vector machine; CTQ, Childhood Trauma Questionnaire; CQ, Cognition Questionnaire; PLSC, Partial Least Squared Correlation analysis; LV, latent variable.*

Results

Descriptive statistics of the whole sample (N=482) are reported in **Table 1**. No significant differences in age, sex, duration of illness, and pharmacological load were observed between MDD and BD. However, BD patients showed a significantly higher number of previous episodes compared to MDD ($q<0.001$). BD and MDD patients were also comparable for HDRS-21, CQ and CTQ domains. HC were younger, with higher level of education and lower CTQ and CQ scores compared to both MDD and BD. In the whole sample, significant and positive correlations were found across all the CTQ and CQ domains (**Figure S1**).

Performances of stratification models

Models based on structural neuroimaging, FC or multimodal data showed good accuracies in clusters' differentiation, identifying two clusters of patients as the optimal clustering solution (accuracy range: 73.4%-84.8%, $q<0.05$). Models trained exclusively on ReHo and fALFF modality did not achieve a predictive accuracy above chance level or significance (**Table 2** and **Figure S2**). The best clustering performance was observed for the FC-based model, showing an accuracy in discriminating clusters of 84.8%. Fleiss' kappa statistic was $k=0.07$, suggesting a low agreement across stratification models in assigning subjects to the same cluster.

Neurobiological characterization of data-driven clusters

All the stratification models distinguished between a cluster of depressed patients with a more preserved brain structure or function and a second one characterized by a more compromised brain signature. Considering the FC-based clusters, Cluster 1 exhibited higher Spos compared to Cluster 2, with the largest effect sizes found in the cingulate gyrus, precuneus, and superior frontal gyrus (SFG). Conversely, Cluster 2 showed overall higher Sneg compared to Cluster 1, despite reduced effect sizes compared to Cluster 1 (**Figure 2**). Similarly, GM and CT-based models uncovered a cluster of depressed patients marked by widespread volumetric reductions and cortical thinning, with the main effects localized in temporo-parietal regions (**Figure S3**). All the DTI-based models uncovered one cluster differing from the second one in opposite direction, with the largest contributions in the corpus callosum and corona radiata (**Figure S4**). When combing all modalities in the multimodal stratification model, clusters' differentiation was mainly guided by DTI measures, with one cluster exhibited higher RD, MD, AD, and lower FA values compared to the other (**Figure S5**).

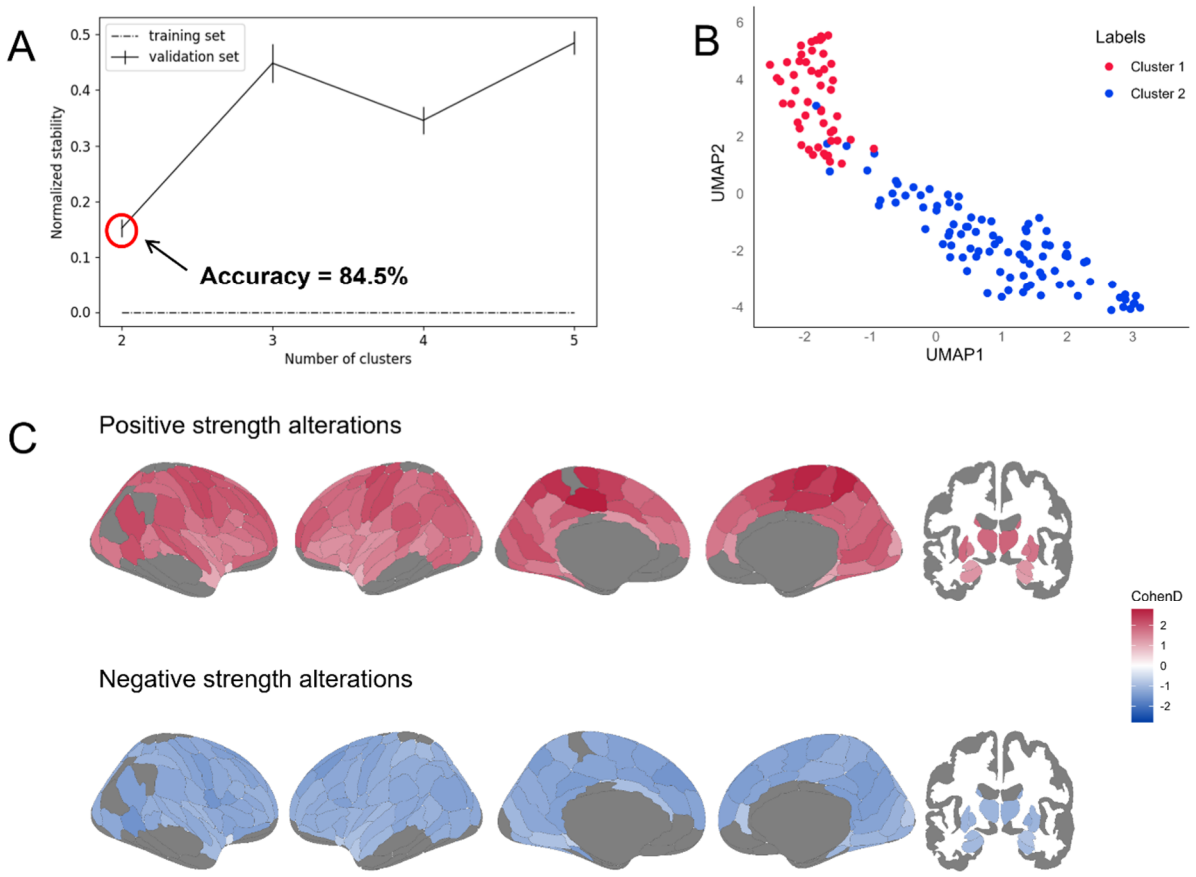

Figure 2. Results of stability-based relative clustering validation on FC strength. *A. Normalized stability plot. Error bars represent the 95% confidence interval for normalized stability from repeated cross-validation. The optimal number of clusters is the one that minimizes the normalized stability. It is clear that the optimal number of clusters is 2 with a normalized stability of 0.15 (i.e., accuracy of 84.5%). B. UMAP plot that shows separated distributions for the discovered clusters. For visualization purposes, Uniform Manifold Approximation and Projection for Dimension Reduction (UMAP) was applied on the original data. C. Cohen's d values describing the magnitude of differences in positive and negative strength values between the FC-based clusters. Positive values (red) indicate higher values for Cluster 1 compared to Cluster 2, whereas negative values (blue) indicate higher values for Cluster 2 compared to Cluster 1. Abbreviations: UMAP, Uniform Manifold Approximation and Projection for Dimension Reduction.*

To clarify the direction of neurobiological alterations in the best-performing stratification model (i.e., FC-based), we examined differences in global and regional Spos and Sneg measures between clusters and HC. At the global level, patients in Cluster 1 showed significantly higher Spos compared to both Cluster 2 and HC, while patients belonging to Cluster 2 exhibited elevated Sneg relative to Cluster 1 and HC (**Figure 3A-B**). Evidence of group differences in Spos or Sneg was also observed across individual brain regions, consistent with the patterns described at the global level (**Table S13**). These results generally indicate that Cluster 1 is distinguished by an increased functional integration, while an abnormal functional segregation characterize Cluster 2.

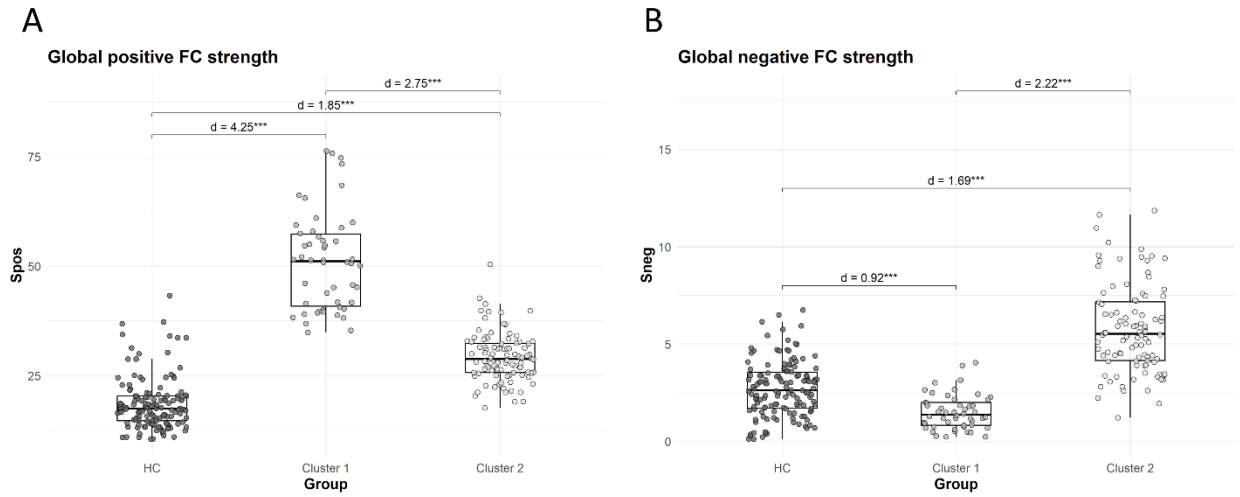

Figure 3. Cluster differences in global positive and negative FC strength compared to healthy controls. *Standardized effect sizes (Cohen's d) are shown for each pairwise group comparison for global positive (A) and negative FC strength (B). Asterisks indicate statistically significant pairwise group comparisons that survive false discovery rate (FDR) q<0.05. Abbreviations: FC, functional connectivity; HC, healthy controls; Sneg, negative functional connectivity strength; Spos, positive functional connectivity strength.*

Differential neurobiological-ACEs associations between clusters

A significant LV pair surviving FDR correction was obtained only for the FC-based model (explained covariance=40.0%, q=0.01) (**Table S11**). The largest BSR were observed for ROIs in the ventral and caudal part of the cingulate gyrus, superior and inferior parietal lobules, insula, somatosensory cortex, as well as the lateral amygdala, thalamus, and basal ganglia, and these effects were found for both Spos and Sneg (**Figure 4A-B**). In Cluster 1 all CTQ domains, except for sexual abuse, significantly contributed to the neurobiological-ACEs multivariate association. The direction of CTQ loadings was negative, meaning that higher exposure to childhood trauma is associated with decreased FC strength. In Cluster 2, negative significant associations emerged for emotional neglect, while positive for sexual abuse. (**Figure 4C**). PLS analysis including HC produced similar results, isolating a significant LV pair (explained covariance=43.0%, q=0.015) (**Table S12**). The contribution of CTQ domains to the neurobiological–ACEs association was highly similar between HC and Cluster 1, whereas only the domains of sexual and physical abuse were significant in Cluster 2. Thus, the identified LV likely reflects a normative neurobiological–ACEs relationship that is present in HC and preserved in Cluster 1, but absent in Cluster 2. (**Figure S6**).

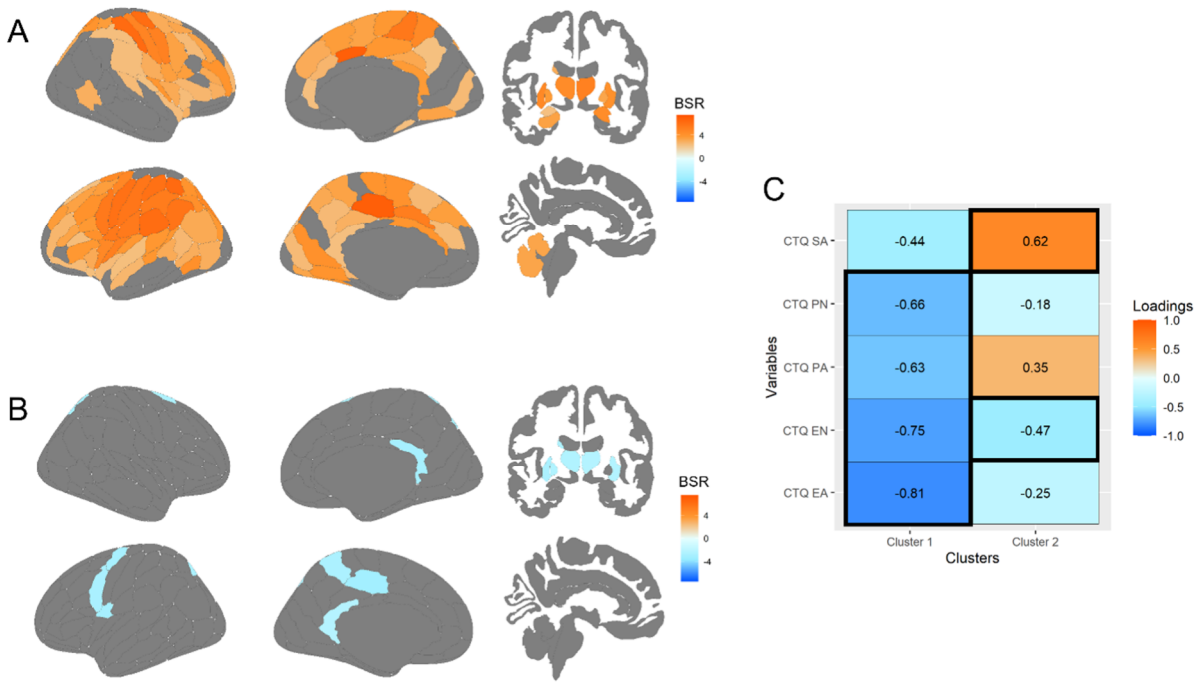

Figure 4. Differences in multivariate brain-ACEs relationships between the FC-based clusters. *A-B. Significant brain bootstrap ratios (BSRs) for positive (A) and negative (B) FC strength in each region. Brain regions with orange BSRs have correlations that have the same directionality shown in the heatmap in (C). Brain regions with blue BSRs have correlations in the opposite direction shown in the heatmap in (C). C. PLS correlations for each CTQ domain (row) and each cluster (columns). Loadings with black outline are those with 95% confidence intervals that do not include zero. Abbreviations: BSR, brain bootstrap ratio; CTQ, Childhood Trauma Questionnaire; SA, sexual abuse; PN, physical neglect; PA, physical abuse; EN, emotional neglect; EA, emotional abuse.*

When considering univariate analyses, patients belonging to the FC-based Cluster 2 showed higher scores in generalization across events and perceived uncontrollability, while a trend toward significance was found for sexual abuse. However, these results did not survive FDR correction (**Table S2**). Compared to HC, both clusters exhibited higher scores in attribution of causality, generalization across events, and CQ total score. However, only Cluster 2 showed higher scores in sexual abuse, CTQ total score, generalization across time, and perceived uncontrollability relative to HC (**Table S10**). At an uncorrected p-values, significant differences in diagnosis were found for clusters derived from AD, while a trend toward significance was detected in the FA-based clusters. No significant differences were detected for clusters derived from GM and CT (**Tables S3-S9**).

Effect of FC strength on cognitive distortions in the FC-based clusters

The final step was to explore whether the LV FC scores differentially mediated the relationships between the LV CTQ scores and CQ domains in the FC-based clusters. Multivariate GLMs did not show significant effects for LV FC scores on CQ domains neither in Cluster 1 (Wilk's λ=0.88, F(5,27)=0.73, p=0.612) nor in Cluster 2 (Wilk's λ=0.87, F(5,58)=1.71, p=0.147). Considering univariate results, LV FC scores significantly and positively predicted generalization across time only in Cluster 2 (b=0.029, p=0.032; overall model fit: R2=0.07, RMSE=0.90, F(1,62)=4.85, p=0.031). Mediation analysis revealed a significant indirect effect of

LV CTQ scores on generalization across time through LV FC scores (i.e., path a*b). The total and the direct effects of LV CTQ scores on generalization across time were not significant; however, the significant indirect effect support the mediation effect of LV FC scores. LV CTQ scores significantly increased LV FC scores (path a), whereas the effect of LV FC scores on generalization across time is marginally significant (path b). These results suggest that in Cluster 2 LV FC scores significantly mediate the relationship between LV CTQ scores and generalization across time, despite the total effect is not significant (**Figure 5**).

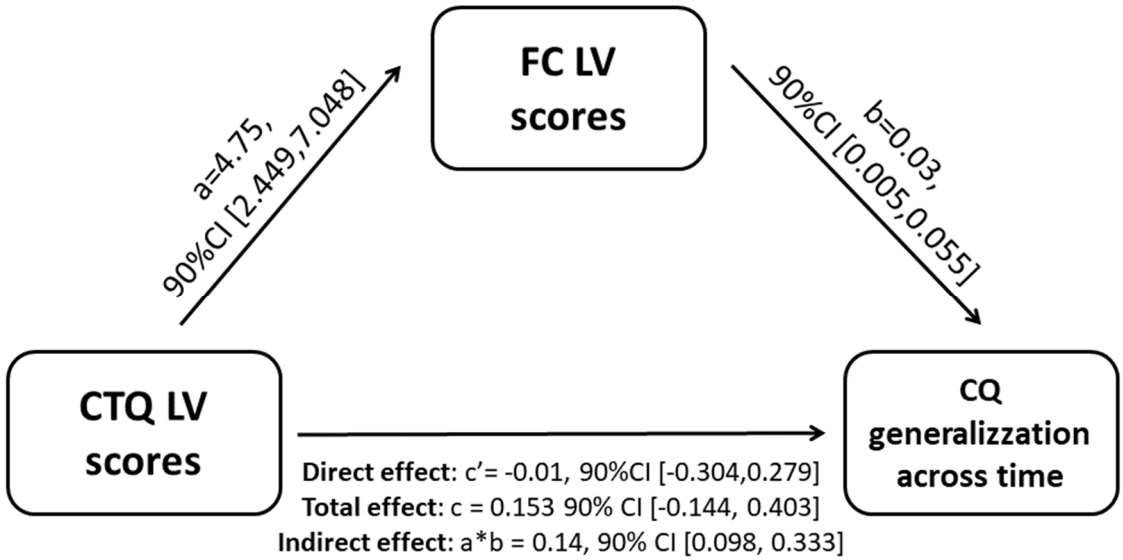

Figure 5. Mediation effect of FC LV scores in the relationship between CTQ LV scores and CQ generalization across time in Cluster 2. *Abbreviations: CQ, cognition questionnaire; CTQ, Childhood Trauma Questionnaire; FC, functional connectivity; LV, latent variable.*

Discussion

This study explored whether multimodal neuroimaging could support clinically meaningful data-driven stratifications of depressive mood disorders. Among all tested models, the highest accuracy was observed for the FC-based model (85%), uncovering two transdiagnostic biotypes: one characterized by widespread high positive FC strength (Cluster 1, N=50), while another one by dominant negative FC strength (Cluster 2, N=96). Importantly, differential neurobiological-ACEs associations emerged. In Cluster 1, childhood trauma was negatively associated with FC in the cingulate gyrus, insula, somatosensory cortex, and subcortical regions, consistent with the ACEs-related pattern also observed in HC. In Cluster 2, emotional neglect was linked to reduced FC, while sexual abuse showed a positive association. ACEs-related FC mediated the relationship between ACEs and NCS of overgeneralization in this latter cluster, supporting biotype-specific neurobiological pathways linking early trauma and cognitive vulnerability.

The functional profiles of the discovered biotypes reflect widespread connectome alterations. While positive correlations may reflect synchronized neural activity, negative correlations have been proposed to indicate longer shortest paths, reflecting less efficient information flow (67). Alterations in the brain connectome are well-documented in psychiatric disorders, possibly representing common neurobiological mechanisms (68–71). Our findings extend this scenario by demonstrating that the unbalance between segregation and integration manifests as distinct biotypes within depression, differing from HC in global and regional FC.

A significant neurobiological-ACEs relationship was differentially present in the two FC biotypes. The regions most affected by ACEs (amygdala, cingulate, thalamus, basal ganglia, insula, sensorimotor areas), are crucial for emotional, cognitive and social functioning, and their functional organization is highly influenced by cortical maturational changes (72–75). The deprivation of adequate emotional stimulation during childhood disrupts these processes by diminishing neurotrophin and neurotransmitters production which, ultimately, end with aberrant neural organization (76,77). Sexual abuse emerged as a key discriminating factor, showing a significant and positive association with FC only in Cluster 2. This association may reflect a compensatory mechanism, consistent with the stress acceleration hypothesis, whereby early adversities accelerate the maturation of brain circuits involved in salience detection and executive functions to promote short-term adaptations (78,79). These findings may point to a more severely affected subgroup, where localized increases in functional coupling compensate for abuse-related widespread connectivity deficits.

The presence of distinct underlying mechanisms is further supported by the mediation analysis, where the ACE-related FC scores mediated the relationship between the ACEs and generalization across time only in the hyper-segregated biotype. Overgeneralization represents a key feature of depressive symptomatology (80), and constitutes a core element of the depressive "cognitive triad" (3). While ACEs are established risk factors for NCS (81–83), these results suggest that the tendency to overgeneralize might characterize a specific neurobiological subtype of depressed patients, which may benefit from cognitive or trauma-focused psychotherapies (84,85).

Structural MRI models did not reveal significant associations with ACEs or NCS, though they reliably distinguished patients with widespread WM dysconnectivity, cortical thinning and volumetric reductions

(accuracies > 70%). These alterations may reflect diagnosis-specific effects, consistent with evidence that GM and DTI metrics differentiate BD and MDD with accuracies up to 78% (86–88). Accordingly, clusters derived from FA and AD exhibited trends toward a significant difference for diagnosis, although not surviving FDR correction. Conversely, this association was not found for the FC-based clusters, suggesting that functional measures are more likely to reflect transdiagnostic signatures rather that clinical diagnoses (28,30,31). Alternatively, the limited overlap with FC clusters may reflect distinct pathological dimensions captured solely by structural modalities, such as immune-inflammatory mechanisms or cognitive deficits (36,89).

The low overlapping between structural and functional clustering solutions might also explain why the multimodal stratification model did not outperform the FC-based one, despite achieving a moderate classification performance (73.4%) and the best internal validity (Silhouette and Davies-Bouldin scores).

Some limitations should be underscored. All patients were inpatients admitted to the same hospital, limiting generalizability. Although pharmacological load was statistically controlled, residual long-lasting effects cannot be completely ruled out. Finally, the modest sample size and lack of additional biological measures (e.g., genetic or inflammatory markers) may have constrained detection of more nuanced associations.

In conclusion, this work shows that FC-based biotypes best captured distinct trauma-related neurobiological profiles in depression. One biotype exhibited hyperconnectivity and negative associations with ACEs; the other, characterized by network segregation, showed a more specific pattern involving sexual abuse, emotional neglect, and overgeneralization. These findings highlight the potential of FC to define transdiagnostic depression subtypes with differential vulnerability to early adversity, informing a neurobiologically grounded taxonomy of mood disorders.

Acknowledgments

This study was supported by the Italian Ministry of Health (grant numbers GR 2019-12370616).

Authors contributions: Conceptualization: BV, FCo. Data curation: FCo, LFU, CM, TC, MA. Formal analysis: FCo, FCa, BB, IB. Funding acquisition: BV. Investigation: FCo. Methodology: BV, FCo. Project administration: BV, SP. Resources: RZ, MC, CC. Software: FCo. Supervision: BV, SP. Visualization: FCo. Writing - original draft preparation: FCo, BV. Writing - review and editing: FCo, FCa, BB, LFU, CM, TC, MA, RZ, CC, MC, CF, AS, IB, FB, SP, BV.

Disclosures

CF was a speaker for Janssen. AS is or was a consultant/speaker for Abbott, Abbvie, Angelini, AstraZeneca, Clinical Data, Boehringer, Bristol-Myers Squibb, Eli Lilly, GlaxoSmithKline, Innovapharma, Italfarmaco, Janssen, Lundbeck, Naurex, Pfizer, Polifarma, Sanofi, Taliaz and Servier. All the other authors declare no financial interests or potential conflicts of interest.

References

1. Cirone C, Secci I, Favole I, Ricci F, Amianto F, Davico C, Vitiello B (2021): What Do We Know about the Long-Term Course of Early Onset Bipolar Disorder? A Review of the Current Evidence. *Brain Sci* 11. https://doi.org/10.3390/brainsci11030341

2. GBD Mental Disorders Collaborators (2022): Global, regional, and national burden of 12 mental disorders in 204 countries and territories, 1990-2019: a systematic analysis for the Global Burden of Disease Study 2019. *Lancet Psychiatry* 9: 137–150.

3. Beck AT (2008): Reviews and Overviews The Evolution of the Cognitive Model of Depression and Its Neurobiological Correlates. *Am J Psychiatry*, vol. 165.

4. Shankman SA, Campbell ML, Klein DN, Leon AC, Arnow BA, Manber R, *et al.* (2013): Dysfunctional attitudes as a moderator of pharmacotherapy and psychotherapy for chronic depression. *J Psychiatr Res* 47: 113–121.

5. Zhou Y, Arend J, Mufson L, Gunlicks-Stoessel M (2021): Change in dysfunctional attitudes and attachment in interpersonal psychotherapy for depressed adolescents. *Psychother Res J Soc Psychother Res* 31: 258–266.

6. Fazakas-DeHoog LL, Rnic K, Dozois DJA (2017): A Cognitive Distortions and Deficits Model of Suicide Ideation. *Eur J Psychol* 13: 178–193.

7. Jones EB, Sharpe L (2017): Cognitive bias modification: A review of meta-analyses. *J Affect Disord* 223: 175–183.

8. Scheepens DS, van Waarde JA, Ten Doesschate F, Westra M, Kroes MCW, Schene AH, *et al.* (2022): Negative cognitive schema modification as mediator of symptom improvement after electroconvulsive therapy in major depressive disorder. *J Affect Disord* 310: 156–161.

9. Spinhoven P, Klein N, Kennis M, Cramer AOJ, Siegle G, Cuijpers P, *et al.* (2018): The effects of cognitive-behavior therapy for depression on repetitive negative thinking: A meta-analysis. *Behav Res Ther* 106: 71–85.

10. Maslej MM, Furukawa TA, Cipriani A, Andrews PW, Sanches M, Tomlinson A, *et al.* (2021): Individual Differences in Response to Antidepressants: A Meta-analysis of Placebo-Controlled Randomized Clinical Trials. *JAMA Psychiatry* 78: 490–497.

11. Kendall KM, Van Assche E, Andlauer TFM, Choi KW, Luykx JJ, Schulte EC, Lu Y (2021): The genetic basis of major depression. *Psychol Med* 51: 2217–2230.

12. Blair D-L, Kingsbury M, Eccles H, Akther A, Siddiqi S, Condran G, *et al.* (2025): Adverse childhood experiences and suicidality in low-income and middle-income countries: a systematic review and meta-analysis. *BMJ Glob Health* 10: e018129.

13. Giampetruzzi E, Tan AC, LoPilato A, Kitay B, Riva Posse P, McDonald WM, *et al.* (2023): The impact of adverse childhood experiences on adult depression severity and treatment outcomes. *J Affect Disord* 333: 233–239.

14. Hayashi Y, Okamoto Y, Takagaki K, Okada G, Toki S, Inoue T, *et al.* (2015): Direct and indirect influences of childhood abuse on depression symptoms in patients with major depressive disorder. *BMC Psychiatry* 15: 244.

15. Teicher MH, Samson JA (2013): Childhood maltreatment and psychopathology: A case for ecophenotypic variants as clinically and neurobiologically distinct subtypes. *Am J Psychiatry* 170: 1114–1133.

16. Teicher MH, Samson JA, Anderson CM, Ohashi K (2016): The effects of childhood maltreatment on brain structure, function and connectivity. *Nat Rev Neurosci* 17: 652–666.

17. Yan L, Kraaijenvanger EJ, Wennekers R, Müller VI, Eickhoff SB, Fernández G, *et al.* (2025): The effects of childhood adversity: Two specific neural patterns. *Neurosci Biobehav Rev* 174: 106176.

18. Benedetti F, Poletti S, Radaelli D, Pozzi E, Giacosa C, Ruffini C, *et al.* (2012): Caudate gray matter volume in obsessive-compulsive disorder is influenced by adverse childhood experiences and ongoing drug treatment. *J Clin Psychopharmacol* 32: 544–547.

19. Benedetti F, Radaelli D, Poletti S, Falini A, Cavallaro R, Dallaspezia S, *et al.* (2011): Emotional reactivity in chronic schizophrenia: structural and functional brain correlates and the influence of adverse childhood experiences. *Psychol Med* 41: 509–519.

20. Benedetti F, Bollettini I, Radaelli D, Poletti S, Locatelli C, Falini A, *et al.* (2014): Adverse childhood experiences influence white matter microstructure in patients with bipolar disorder. *Psychol Med* 44: 3069–3082.

21. Poletti S, Vai B, Smeraldi E, Cavallaro R, Colombo C, Benedetti F (2016): Adverse childhood experiences influence the detrimental effect of bipolar disorder and schizophrenia on cortico-limbic grey matter volumes. *J Affect Disord* 189: 290–297.

22. Poletti S, Aggio V, Brioschi S, Bollettini I, Falini A, Colombo C, Benedetti F (2018): Impact of early and recent stress on white matter microstructure in major depressive disorder. *J Affect Disord* 225: 289–297.

23. Poletti S, Locatelli C, Radaelli D, Lorenzi C, Smeraldi E, Colombo C, Benedetti F (2014): Effect of early stress on hippocampal gray matter is influenced by a functional polymorphism in EAAT2 in bipolar disorder. *Prog Neuropsychopharmacol Biol Psychiatry* 51: 146–152.

24. Bzdok D, Meyer-Lindenberg A (2018, March): Machine Learning for Precision Psychiatry: Opportunities and Challenges. *Biological Psychiatry: Cognitive Neuroscience and Neuroimaging*, vol. 3. Elsevier Inc, pp 223–230.

25. Fernandes BS, Williams LM, Steiner J, Leboyer M, Carvalho AF, Berk M (2017): The new field of "precision

psychiatry." *BMC Med* 15. https://doi.org/10.1186/s12916-017-0849-x

26. Tiego J, Martin EA, DeYoung CG, Hagan K, Cooper SE, Pasion R, *et al.* (2023): Precision behavioral phenotyping as a strategy for uncovering the biological correlates of psychopathology. *Nat Ment Health* 1: 304–315.

27. Xie C, Xiang S, Shen C, Peng X, Kang J, Li Y, *et al.* (2023): A shared neural basis underlying psychiatric comorbidity. *Nat Med* 29: 1232–1242.

28. Goldstein-Piekarski AN, Ball TM, Samara Z, Staveland BR, Keller AS, Fleming SL, *et al.* (2022): Mapping Neural Circuit Biotypes to Symptoms and Behavioral Dimensions of Depression and Anxiety. *Biol Psychiatry* 91: 561–571.

29. Williams LM (2016): Precision psychiatry: a neural circuit taxonomy for depression and anxiety. *Lancet Psychiatry* 3: 472–480.

30. Williams LM (2017): Defining biotypes for depression and anxiety based on large-scale circuit dysfunction: a theoretical review of the evidence and future directions for clinical translation. *Depress Anxiety* 34: 9–24.

31. Tozzi L, Zhang X, Pines A, Olmsted AM, Zhai ES, Anene ET, *et al.* (2024): Personalized brain circuit scores identify clinically distinct biotypes in depression and anxiety. *Nat Med* 30: 2076–2087.

32. Drysdale AT, Grosenick L, Downar J, Dunlop K, Mansouri F, Meng Y, *et al.* (2017): Resting-state connectivity biomarkers define neurophysiological subtypes of depression. *Nat Med* 23: 28–38.

33. Liang S, Deng W, Li X, Greenshaw AJ, Wang Q, Li M, *et al.* (2020): Biotypes of major depressive disorder: Neuroimaging evidence from resting-state default mode network patterns. *NeuroImage Clin* 28. https://doi.org/10.1016/j.nicl.2020.102514

34. Price RB, Gates K, Kraynak TE, Thase ME, Siegle GJ (2017): Data-Driven Subgroups in Depression Derived from Directed Functional Connectivity Paths at Rest. *Neuropsychopharmacology* 42: 2623–2632.

35. Tokuda T, Yoshimoto J, Shimizu Y, Okada G, Takamura M, Okamoto Y, *et al.* (2018): Identification of depression subtypes and relevant brain regions using a data-driven approach. *Sci Rep* 8: 14082.

36. Colombo F, Calesella F, Bravi B, Fortaner-Uyà L, Monopoli C, Tassi E, *et al.* (2024): Multimodal brain-derived subtypes of Major depressive disorder differentiate patients for anergic symptoms, immune-inflammatory markers, history of childhood trauma and treatment-resistance. *Eur Neuropsychopharmacol* 85: 45–57.

37. Sha Z, Wager TD, Mechelli A, He Y (2019): Common Dysfunction of Large-Scale Neurocognitive Networks Across Psychiatric Disorders. *Biol Psychiatry* 85: 379–388.

38. Hamilton M (1986): The Hamilton rating scale for depression. *Assessment of Depression*. Springer, pp 143–152.

39. Sackeim HA (2001): The definition and meaning of treatment-resistant depression. *J Clin Psychiatry* 62: 10–17.

40. Bernstein DP, Stein JA, Newcomb MD, Walker E, Pogge D, Ahluvalia T, *et al.* (2003): Development and validation of a brief screening version of the Childhood Trauma Questionnaire. *Child Abuse Negl* 27: 169–190.

41. Fennell MJV, Campbell EA (1984): The cognitions questionnaire: Specific thinking errors in depression. *Br J Clin Psychol* 23: 81–92.

42. Gaser C, Dahnke R, Thompson PM, Kurth F, Luders E, the Alzheimer's Disease Neuroimaging Initiative (2024): CAT: a computational anatomy toolbox for the analysis of structural MRI data. *GigaScience* 13: giae049.

43. Desikan RS, Ségonne F, Fischl B, Quinn BT, Dickerson BC, Blacker D, *et al.* (2006): An automated labeling system for subdividing the human cerebral cortex on MRI scans into gyral based regions of interest. *NeuroImage* 31: 968–980.

44. Smith SM, Jenkinson M, Woolrich MW, Beckmann CF, Behrens TEJ, Johansen-Berg H, *et al.* (2004): Advances in functional and structural MR image analysis and implementation as FSL. *Neuroimage* 23: S208–S219.

45. Smith SM, Jenkinson M, Johansen-Berg H, Rueckert D, Nichols TE, Mackay CE, *et al.* (2006): Tract-based spatial statistics: Voxelwise analysis of multi-subject diffusion data. *NeuroImage* 31: 1487–1505.

46. Woolrich MW, Jbabdi S, Patenaude B, Chappell M, Makni S, Behrens T, *et al.* (2009): Bayesian analysis of neuroimaging data in FSL. *Neuroimage* 45: S173-86.

47. Horsfield MA (1999): Mapping eddy current induced fields for the correction of diffusion-weighted echo planar images. *Magn Reson Imaging* 17: 1335–1345.

48. Smith SM (2002): Fast robust automated brain extraction. *Hum Brain Mapp* 17: 143–155.

49. Mori S, Oishi K, Jiang H, Jiang L, Li X, Akhter K, *et al.* (2008): Stereotaxic white matter atlas based on diffusion tensor imaging in an ICBM template. *NeuroImage* 40: 570–582.

50. Waller L, Erk S, Pozzi E, Toenders YJ, Haswell CC, Büttner M, *et al.* (2022): ENIGMA HALFPIPE : Interactive, reproducible, and efficient analysis for resting-state and task-based FMRI data. *Hum Brain Mapp* 43: 2727–2742.

51. Pruim RH, Mennes M, Buitelaar JK, Beckmann CF (2015): Evaluation of ICA-AROMA and alternative strategies for motion artifact removal in resting state fMRI. *Neuroimage* 112: 278–287.

52. Pruim RH, Mennes M, van Rooij D, Llera A, Buitelaar JK, Beckmann CF (2015): ICA-AROMA: A robust ICA-based strategy for removing motion artifacts from fMRI data. *Neuroimage* 112: 267–277.

53. Muschelli J, Nebel MB, Caffo BS, Barber AD, Pekar JJ, Mostofsky SH (2014): Reduction of motion-related artifacts

in resting state fMRI using aCompCor. *Neuroimage* 96: 22–35.

54. Fan L, Li H, Zhuo J, Zhang Y, Wang J, Chen L, *et al.* (2016): The human brainnetome atlas: a new brain atlas based on connectional architecture. *Cereb Cortex* 26: 3508–3526.

55. Buckner RL, Krienen FM, Castellanos A, Diaz JC, Yeo BT (2011): The organization of the human cerebellum estimated by intrinsic functional connectivity. *J Neurophysiol* 106: 2322–2345.

56. Zou Q-H, Zhu C-Z, Yang Y, Zuo X-N, Long X-Y, Cao Q-J, *et al.* (2008): An improved approach to detection of amplitude of low-frequency fluctuation (ALFF) for resting-state fMRI: fractional ALFF. *J Neurosci Methods* 172: 137–141.

57. Zang Y, Jiang T, Lu Y, He Y, Tian L (2004): Regional homogeneity approach to fMRI data analysis. *Neuroimage* 22: 394–400.

58. Johnson WE, Li C, Rabinovic A (2007): Adjusting batch effects in microarray expression data using empirical Bayes methods. *Biostatistics* 8: 118–127.

59. Landi I, Mandelli V, Lombardo MV (2021): reval: A Python package to determine best clustering solutions with stability-based relative clustering validation. *Patterns* 2. https://doi.org/10.1016/j.patter.2021.100228

60. Lange T, Roth V, Braun ML, Buhmann JM (n.d.): *Stability-Based Validation of Clustering Solutions*.

61. Alfaro-Almagro F, McCarthy P, Afyouni S, Andersson JLR, Bastiani M, Miller KL, *et al.* (2021): Confound modelling in UK Biobank brain imaging. *Neuroimage* 224: 117002.

62. Kumar A, Daumé H (2011): A co-training approach for multi-view spectral clustering. 393–400.

63. Liu Y, Hayes DN, Nobel A, Marron JS (2008): Statistical significance of clustering for high-dimension, low-sample size data. *J Am Stat Assoc* 103: 1281–1293.

64. Krishnan A, Williams LJ, McIntosh AR, Abdi H (2011): Partial Least Squares (PLS) methods for neuroimaging: A tutorial and review. *NeuroImage* 56: 455–475.

65. Kebets V, Holmes AJ, Orban C, Tang S, Li J, Sun N, *et al.* (2019): Somatosensory-Motor Dysconnectivity Spans Multiple Transdiagnostic Dimensions of Psychopathology. *Biol Psychiatry* 86: 779–791.

66. Hayes AF (2012): PROCESS : A Versatile Computational Tool for Observed Variable Mediation , Moderation , and Conditional Process Modeling 1.

67. Chen G, Chen G, Xie C, Li S-J (2011): Negative functional connectivity and its dependence on the shortest path length of positive network in the resting-state human brain. *Brain Connect* 1: 195–206.

68. de Lange SC, Scholtens LH, van den Berg LH, Boks MP, Bozzali M, Cahn W, *et al.* (2019): Shared vulnerability for

connectome alterations across psychiatric and neurological brain disorders. *Nat Hum Behav* 3: 988–998.

69. Hansen JY, Shafiei G, Vogel JW, Smart K, Bearden CE, Hoogman M, *et al.* (2022): Local molecular and global connectomic contributions to cross-disorder cortical abnormalities. *Nat Commun* 13: 4682.

70. Repple J, Gruber M, Mauritz M, de Lange SC, Winter NR, Opel N, *et al.* (2023): Shared and Specific Patterns of Structural Brain Connectivity Across Affective and Psychotic Disorders. *Biol Psychiatry* 93: 178–186.

71. Xia M, Womer FY, Chang M, Zhu Y, Zhou Q, Edmiston EK, *et al.* (2019): Shared and Distinct Functional Architectures of Brain Networks Across Psychiatric Disorders. *Schizophr Bull* 45: 450–463.

72. Casey BJ, Heller AS, Gee DG, Cohen AO (2019): Development of the emotional brain. *Neurosci Lett* 693: 29–34.

73. Dong H-M, Zhang X-H, Labache L, Zhang S, Ooi LQR, Yeo BTT, *et al.* (2024): Ventral attention network connectivity is linked to cortical maturation and cognitive ability in childhood. *Nat Neurosci*. https://doi.org/10.1038/s41593-024-01736-x

74. Luo AC, Sydnor VJ, Pines A, Larsen B, Alexander-Bloch AF, Cieslak M, *et al.* (2024): Functional connectivity development along the sensorimotor-association axis enhances the cortical hierarchy. *Nat Commun* 15: 3511.

75. Park S, Haak KV, Oldham S, Cho H, Byeon K, Park B, *et al.* (2024): A shifting role of thalamocortical connectivity in the emergence of cortical functional organization. *Nat Neurosci* 27: 1609–1619.

76. De Bellis MD (2005): The psychobiology of neglect. *Child Maltreat* 10: 150–172.

77. van der Kolk BA (2003): The neurobiology of childhood trauma and abuse. *Child Adolesc Psychiatr Clin* 12: 293–317.

78. Callaghan BL, Tottenham N (2016): The Stress Acceleration Hypothesis: Effects of early-life adversity on emotion circuits and behavior. *Curr Opin Behav Sci* 7: 76–81.

79. Holz NE, Berhe O, Sacu S, Schwarz E, Tesarz J, Heim CM, Tost H (2023): Early Social Adversity, Altered Brain Functional Connectivity, and Mental Health. *Biol Psychiatry* 93: 430–441.

80. Gamble B, Moreau D, Tippett LJ, Addis DR (2019): Specificity of Future Thinking in Depression: A Meta-Analysis. *Perspect Psychol Sci* 14: 816–834.

81. Alaftar İ, Uzer T (2022): Understanding intergenerational transmission of early maladaptive schemas from a memory perspective: Moderating role of overgeneral memory on adverse experiences. *Child Abuse Negl* 127: 105539.

82. Mansueto G, Cavallo C, Palmieri S, Ruggiero GM, Sassaroli S, Caselli G (2021, May): Adverse childhood experiences and repetitive negative thinking in adulthood: A systematic review. *Clinical Psychology and Psychotherapy*, vol. 28. John Wiley and Sons Ltd, pp 557–568.

83. Poletti S, Colombo C, Benedetti F (2014): Adverse childhood experiences worsen cognitive distortion during adult bipolar depression. *Compr Psychiatry* 55: 1803–1808.

84. Cohen JA, Mannarino AP (2015): Trauma-focused Cognitive Behavior Therapy for Traumatized Children and Families. *Child Adolesc Psychiatr Clin N Am* 24: 557–70.

85. Wiles N, Thomas L, Abel A, Ridgway N, Turner N, Campbell J, *et al.* (2013): Cognitive behavioural therapy as an adjunct to pharmacotherapy for primary care based patients with treatment resistant depression: results of the CoBalT randomised controlled trial. *The Lancet* 381: 375–384.

86. Calesella F, Colombo F, Bravi B, Fortaner-Uyà L, Monopoli C, Poletti S, *et al.* (2024): A machine learning pipeline for efficient differentiation between bipolar and major depressive disorder based on multimodal structural neuroimaging. *Neurosci Appl* 3: 103931.

87. Colombo F, Calesella F, Mazza MG, Melloni EMT, Morelli MJ, Scotti GM, *et al.* (2022): Machine learning approaches for prediction of bipolar disorder based on biological, clinical and neuropsychological markers: A systematic review and meta-analysis. *Neurosci Biobehav Rev* 135. https://doi.org/10.1016/j.neubiorev.2022.104552

88. Vai B, Parenti L, Bollettini I, Cara C, Verga C, Melloni E, *et al.* (2020): Predicting differential diagnosis between bipolar and unipolar depression with multiple kernel learning on multimodal structural neuroimaging. *Eur Neuropsychopharmacol* 34: 28–38.

89. Liang S, Wang Q, Kong X, Deng W, Yang X, Li X, *et al.* (2019): White Matter Abnormalities in Major Depression Biotypes Identified by Diffusion Tensor Imaging. *Neurosci Bull* 35: 867–876.

Tables

Table 1. Descriptive statistics of the whole sample. Results are reported as mean ± standard deviation for continuous variables, whereas frequencies are reported for categorical variables. Abbreviations: HC, Healthy Controls; MDD, Major Depressive Disorder; BD, Bipolar Disorder; HDRS-21, Hamilton Depression Rating Scale – 21 items; CTQ, Childhood Trauma Questionnaire; CQ, Cognition Questionnaire. [a]subsample of N=327 (MDD=106; BD=123; HC=98); [b]subsample of N=258 (MDD=87; BD=121; HC=50); *FDR-corrected q<0.05.

Variable	HC (N=138)	MDD (N=135)	BD (N=209)	F / χ2	p	pFDR	Post-hoc
Age	30.75±10.6	49.39±9.95	47.39±10.6	139.09	<0.001	<0.001*	MDD>HC BD>HC
Sex	77 F; 61 M	95 F; 40 M	133 F; 76 M	6.26	0.04	0.06	
Scanner	0 Gyroscan; 138 Igenia	48 Gyroscan; 87 Igenia	144 Gyroscan; 65 Igenia	166.07	<0.001	<0.001*	
No. of episodes	/	5.24±5.58	12.61±12.96	38.92	<0.001	<0.001*	BD>MDD
Age at onset	/	32.63±11.39	29.21±10.05	8.57	<0.001	0.01*	MDD>BD
Duration of illness (years)	/	16.76±10.52	18.18±10.96	1.42	0.23	0.26	
Years of education	16.51±3.04	12.86±3.9	11.88±3.78	69.82	<0.001	<0.001*	HC>MDD HC>BD MDD>BD
Pharmacological load	/	4.75±2.29	4.5±2.17	1.05	0.31	0.32	
HDRS-21 total score	/	22.48±6.99	22.43±4.85	0.01	0.93	0.93	
CTQ physical abuse[a]	5.62±1.58	6.55±4.37	5.96±2.07	2.64	0.07	0.09	
CTQ emotional abuse[a]	8.04±3.59	8.99±4.24	8.11±3.5	2.08	0.13	0.15	
CTQ sexual abuse[a]	5.06±0.78	6.04±2.96	5.63±1.88	5.61	<0.001	0.01*	MDD>HC BD>HC
CTQ physical neglect[a]	6.58±2.74	7.7±3.36	6.76±2.46	4.62	0.01	0.02*	MDD>HC MDD>BD
CTQ emotional neglect[a]	11.1±4.56	12.93±4.98	12.43±4.9	3.90	0.02	0.03*	MDD>HC MDD>BD
CTQ total score[a]	36.77±10.07	43.39±13.09	40.85±14.59	6.82	<0.001	<0.001*	MDD>HC BD>HC

CQ emotional impact[b]	3.04±3.17	4.17±2.61	4.18±3.02	3.06	0.05	0.06	
CQ attribution of causality[b]	3.5±2.2	4.93±2.34	5.5±2.57	12.08	<0.001	<0.001*	MDD>HC BD>HC
CQ generalization across time[b]	2.74±1.83	4.21±2.89	4.64±3.03	8.23	<0.001	<0.001*	MDD>HC BD>HC
CQ generalizzation across events[b]	3.76±2.51	6.15±2.9	6.26±3.05	14.43	<0.001	<0.001*	MDD>HC BD>HC
CQ perceived uncontrollability[b]	2.68±2.05	3.54±2.63	4.1±2.76	5.38	0.01	0.01*	BD>HC
CQ total score[b]	14.26±7.71	23±10.4	24.64±11.2	18.33	<0.001	<0.001*	MDD>HC BD>HC

Table 2. Clustering models' performance. For each feature, number of clusters, normalized stability measures, and accuracies (in percentage) are reported. For comparison, the number of clusters identified based on internal measures (i.e., Silhouette and Davies-Bouldin scores) are reported in brackets. Models are sorted based on normalized stability measures, where lower values indicate a more stable clustering solution. FDR-corrected q-values obtained from 10,000 Monte-Carlo simulations are reported. Abbreviations: Acc, accuracy; Sil, Silhouette score; DB, Davies-Bouldin score; FC, functional connectivity; GM, grey matter; CT, cortical thickness; RD, radial diffusivity; FA, fractional anisotropy; AD, axial diffusivity; MD, mean diffusivity; ReHo, regional homogeneity; fALFF, fractional amplitude of low frequency fluctuations; SVM, support vector machine. *FDR-corrected q<0.05.

Model	**Algorithms**	**Clusters**	**Stability (error)**	**Acc**	**Sil**	**DB**	**q**
FC	Kmeans + SVM	2	0.15(0.02)	84.8	0.29(2)	1.24(2)	<0.001*
GM	Kmeans + SVM	2	0.17(0.01)	83.2	0.14(2)	2.14(2)	<0.001*
CT	Kmeans + SVM	2	0.18(0.02)	81.9	0.27(2)	1.51(2)	<0.001*
RD	Kmeans + SVM	2	0.20(0.02)	80.1	0.17(2)	1.90(2)	0.002*
FA	Kmeans + SVM	2	0.21(0.01)	79.2	0.20(2)	1.73(2)	<0.001*
AD	Kmeans + SVM	2	0.21(0.01)	78.8	0.15(2)	2.11(2)	<0.001*
MD	Kmeans + SVM	2	0.24(0.02)	76.5	0.20(2)	1.84(2)	0.04*
Multimodal	Multiview + SVM	2	0.27(0.04)	73.4	0.49(2)	0.76(2)	0.002*
ReHo	Kmeans + SVM	2	0.59(0.04)	40.9	0.07(2)	3.21(3)	0.044*
fALFF	Kmeans + SVM	3	0.67(0.03)	31.6	0.10(2)	3.04(5)	0.852